

RSC Advances



This is an *Accepted Manuscript*, which has been through the Royal Society of Chemistry peer review process and has been accepted for publication.

Accepted Manuscripts are published online shortly after acceptance, before technical editing, formatting and proof reading. Using this free service, authors can make their results available to the community, in citable form, before we publish the edited article. This *Accepted Manuscript* will be replaced by the edited, formatted and paginated article as soon as this is available.

You can find more information about *Accepted Manuscripts* in the [Information for Authors](#).

Please note that technical editing may introduce minor changes to the text and/or graphics, which may alter content. The journal's standard [Terms & Conditions](#) and the [Ethical guidelines](#) still apply. In no event shall the Royal Society of Chemistry be held responsible for any errors or omissions in this *Accepted Manuscript* or any consequences arising from the use of any information it contains.

Cite this: DOI: 10.1039/c0xx00000x

www.rsc.org/xxxxxx

ARTICLE TYPE

Magnetically recoverable mesoporous melamine–formaldehyde nanoparticles as an efficient adsorbent for hexavalent chromium removal

Zhongfei Lv,^a Dandan Zhao,^b Changsheng Liang,^a Jiayang Cui,^a Yangben Cai^a and Shiai Xu^{*a}⁵ Received (in XXX, XXX) Xth XXXXXXXXX 20XX, Accepted Xth XXXXXXXXX 20XX

DOI: 10.1039/b000000x

Functional porous nanoparticles have been considered as potential adsorbents for chromium (Cr) removal due to their unique properties such as high surface area, nanosized structure and specific affinity for heavy metal ions. Among these adsorbents, magnetic supports are one of the most efficient adsorbents for their unique advantages of easy separation under external magnetic fields. In this study, magnetic mesoporous melamine–formaldehyde (MMMf) nanoparticles with high surface area (393 m²/g), uniform pore sizes (6.9 nm), and relatively high saturation magnetization (4.3 emu/g) have been prepared. These MMMf nanoparticles are highly effective in removing toxic hexavalent chromium (Cr (VI)) from water within 5 to 10 min. More importantly, they can be easily regenerated by a simple basic treatment (0.1 M NaOH) and reused for at least five times. The effects of initial Cr (VI) concentration, temperature and pH on the adsorption properties of MMMf are also investigated. The superior adsorption properties of MMMf make them to be an attractive adsorbent for water quality purification and improvement.

1. Introduction

Water quality has been deteriorating because of sustained population growth, industrialization, agricultural activities, and geological or environmental changes.^{1–4} A variety of organic and inorganic chemicals, physical and biological pollutants have been reported to be water contaminants.⁵ In particular, exposure to heavy metal ions, even at a trace level, is believed to be a risk for human beings.^{6–8} Hexavalent chromium (Cr (VI)) has long been regarded as one of the most hazardous wastes for its wide existence and strong oxidation property, which may trigger vomiting, gastric ulceration, lung cancer, and liver damage in human beings.^{9–11} The United States Environmental Protection Agency (US EPA) has stipulated that the concentration of Cr (VI) discharged to surface water must be lower than 0.05 mg L⁻¹.^{12,13} New and innovative methods are of great importance to devise technologies to address chromium pollution, with adsorption likely being the most common method in practical use.^{14–19} Thus, there is a strong demand for the development of efficient Cr (VI) adsorbents with high adsorption capacity, fast adsorption kinetics, easy separation and regeneration.

Magnetic supports (nanospheres, nanoparticles, and nanocomposites) have been considered as potential adsorbents for Cr removal due to their unique advantage of easy separation under external magnetic fields.^{20–22} However, most magnetic oxides such as γ -Fe₂O₃ and Fe₃O₄ exhibit a relatively small surface area and few functional groups, thus limiting their abilities to trap metal ions.^{23–26} Moreover, the most commonly used magnetic adsorbents are based on iron oxides and thus particularly susceptible to leaching under acidic conditions.

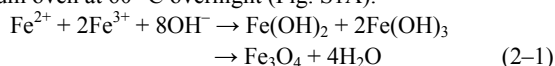
Because mesoporous silica with an accessible pore size, high surface area, pore volume, and acid resistance is favorable for the loading and diffusion of functionalized nanomaterials, the integration of mesoporous silica with magnetic iron oxide nanoparticles is undoubtedly a great advance for practical applications.^{27–31} However, surface modification including physical coating and covalent binding is also needed to further facilitate the adsorption affinity.^{32–34}

To obtain an adsorbent with higher adsorption capacity, better selectivity, and reusability for Cr (VI) removal, we designed and synthesized magnetic mesoporous melamine–formaldehyde (MMMf) nanoparticles. Specifically, magnetic Fe₃O₄ nanospheres coated with a thin layer of mesoporous SiO₂ (denoted as Fe₃O₄@SiO₂) were adopted as the inside material, and mesoporous melamine–formaldehyde resins (MMF), which were demonstrated to be an effective adsorbent for Cr (VI) in our previous study³⁵ were organized into the external layer (denoted as Fe₃O₄@SiO₂@MMF). It is noteworthy that the magnetic core Fe₃O₄ of MMMf is smaller than that of most reported magnetic oxides, which favors to obtain an adsorbent with a thick functional layer. Thus, when using the same mass adsorbent, this adsorbent has more functional groups to catch Cr (VI) compared with some big core magnetic adsorbent. Moreover, the mesoporous silicon with higher surface area could not only decrease the leaching of iron ions in acid solution, but also enhance the surface area of MMMf. These special structural properties allow MMMf to have higher adsorption capacity and selectivity for Cr (VI), and to be reused at least five times, which may dramatically enhance the efficiency of wastewater treatment and reduce the treatment cost to a large extent.

2. Experiment

2.1 Synthesis of Fe₃O₄ nanospheres

Magnetic Fe₃O₄ nanospheres were prepared through co-precipitating Fe²⁺ and Fe³⁺ ions using ammonia solution as reported previously.³⁶ The ferric chloride and ferrous sulfate at a molar ratio of 2:1 were dissolved in water under a N₂ atmosphere. Chemical precipitation was achieved at 40 °C under vigorous stirring by adding 29 wt.% NH₄OH solution. During the reaction process (2–1), pH was maintained at approximately 10 and the precipitates were heated at 80 °C for 30 min. Finally, the products were washed several times with water and ethanol, and dried in a vacuum oven at 60 °C overnight (Fig. S1A).



2.2 Synthesis of Fe₃O₄@SiO₂ nanocomposites

The Fe₃O₄@SiO₂ nanocomposites were prepared via a solvothermal method.³⁷ In a typical process, 0.1 g of F127 and 3.0 g of boric acid (1.3 M) were first dissolved in 40 mL of deionized water, then 0.15 g of Fe₃O₄ nanospheres were added into the aqueous solution and homogenized ultrasonically to form a uniform dispersion. Then, 0.46 g of tetraethyl orthosilicate (TEOS) was injected dropwise into the solution under vigorous mechanical agitation in a water bath at 40 °C for 24 h, and then the solution was transferred into a 50 mL autoclave and maintained at 100 °C for 24 h. Finally, the products were collected with a magnet and washed several times with ethanol and water before being dried in vacuum at 40 °C for 6 h. The final products Fe₃O₄@SiO₂ nanocomposites were obtained after being calcined in atmosphere at 550 °C for 5 h to remove the copolymer templates.

2.3 Synthesis of MMMFS (Fe₃O₄@SiO₂@MMF)

MMMF was hydrothermally synthesized from a mixture of melamine, (HCHO)_n, F127, NaOH, H₂O and Fe₃O₄@SiO₂ at a molar ratio of 1.0: 3.0: 0.002: 0.042: 18.0: X at 150 °C for 24 h. As a typical run, 7.56 g of melamine, 5.40 g of paraformaldehyde and 0.10 g of NaOH were dissolved in 20 mL of deionized water and stirred at 80 °C for 15 min. Another 20 mL of deionized water containing 1.50 g of F127, 3.5 mL of 36 wt. % HCl and 0.75 g of Fe₃O₄@SiO₂ aqueous solution was added, and the mixture was ultrasonically treated to form a uniform dispersion. The mixture was stirred at room temperature for at least 2 h and then transferred to an autoclave and heated at 150 °C for 24 h. After filtrating, washing and drying, a maroon solid was finally obtained (Fig. S1C). F127 was removed by extraction with ethanol at 60 °C for 3 h.

2.4 Adsorption experiments

Batch adsorption experiments were conducted by adding 0.05 g of MMMF to 50 mL of different Cr (VI) test solutions (45.7, 83.3, 113.9, and 175.7 ppm) at different pH values (2–12) and temperatures (20, 25, 30, 35 and 40 °C) in a 100 mL Erlenmeyer flask. The initial pH of the solution was adjusted using 0.1 M HCl or 0.1 M NaOH. The mixture was stirred at 150 rpm for 1 – 60 min. MMMF was separated from the test solution by a magnetic field, and the amount of Cr (VI) adsorbed was calculated from the difference between its concentration in the test solution and the

supernatant liquid, which was determined by furnace atomic absorption spectrometry (FAAS).

The amount of metal adsorbed (mg) per unit mass of MMMF, q_t , was calculated using the following equation.

$$q_t = \frac{V(c_0 - c_t)}{m} \quad (1)$$

Here, q_t is the adsorption capacity of MMMF (mg/g), c_0 and c_t are the initial and equilibrium Cr (VI) concentration (mg/L), m is the mass of adsorbent (g), V is the solution volume (L), and t is the contact time (min).

2.5 Desorption experiments

In these experiments, 50 mL of 0.1 M NaOH was added as the eluent to a 100 mL Erlenmeyer flask containing 0.05 g of MMMF/Cr (MMMF adsorbed Cr). The mixture was stirred at 150 rpm for 1 – 60 min. MMMF/Cr was separated from the test solution by a magnetic field. The amount of Cr (VI) desorbed was calculated from the difference between the adsorption capacity of MMMF and the final concentration of Cr (VI) ions in the desorption medium. The initial solution and supernatant liquid of Cr (adsorbed and desorbed medium) were analyzed by FAAS.

The desorption percentages of Cr (VI) ions from MMMF/Cr were calculated from the amount of Cr (VI) ions adsorbed and the final concentration of Cr (VI) ions in the desorption medium using the following equation:

$$\text{desorption (\%)} = \frac{c_t'}{c_0 - c_t} \quad (2)$$

Here, *desorption (%)* is the percentage of desorption and c_t' is the concentration of desorption (mg/L).

2.6 Characterizations

Field-emission scanning electron microscopy (FESEM) images were obtained using a S4800 scanning electron microscope (Hitachi, Japan). Before the measurement, the samples were sprayed with a film of gold dust. The chemical compositions of MMMF and MMMF/Cr were determined using energy dispersive spectrometer (EDS; QUANTAX 400–30). High-resolution images were obtained using a JEM–2100F transmission electron microscope (TEM, Japan) operated at an accelerating voltage of 200 kV and equipped with a charge-coupled device camera. N₂ sorption isotherms were measured on a Micromeritics ASAP 2460 system (USA) at liquid nitrogen temperature (–196 °C). The samples were outgassed for 10 h at 150 °C before the measurements. The apparent surface area was calculated using the Brunauer–Emmett–Teller (BET) method. The pore size distribution was evaluated by Barrett–Joyner–Halenda (BJH) method using the adsorption branch, and the pore volume of mesopores was calculated from the amount of nitrogen adsorbed at P/P₀ = 0.99. ¹³C MAS NMR spectra were obtained using a Bruker Avance–400 spectrometer (Switzerland) operating at 100.6 MHz for ¹³C using a Bruker 4 mm double resonance probe–head operating at a spinning rate of 10 kHz. Fourier transform infrared (FTIR) were obtained using a Nicolet 6700 FTIR spectrometer (USA) in the range of 400–4000 cm^{–1} and recorded on solid samples in a KBr matrix. Thermo gravimetric analysis (TGA) was performed on a STA449C thermal analyzer (German) with a heating rate of 5 °C/min at nitrogen atmosphere.

Wide-angle X-ray diffraction (WXR) patterns were recorded on a Rigaku D/max 2550v X-ray diffractometer (Japan) with Cu K α radiation ($\lambda = 1.5418 \text{ \AA}$) and 2θ ranging from 10° to 90° . The magnetization curves were measured using a vibrating sample magnetometer (VSM, LakeShore, USA model 7407) at room temperature. The powder was placed in a teflon sample holder for the mass measured. The mass magnetization, M (emu/g), was measured for different applied magnetic fields up to $B = 0.4$ Tesla. The concentration of the Cr (VI) solution was measured by FAAS on a novAA (German). Inductively coupled plasma (ICP Agilent 725ES) was used to analyze the concentration of iron ions.

3. Results and Discussion

3.1 Adsorbent characterizations

The synthetic procedure of MMMF is presented in Fig. 1A. Firstly, magnetic Fe_3O_4 nanospheres of approximately 10 to 40 nm in diameter (Fig. 1B, D; Fig. S2) are coated with a thin layer of mesoporous SiO_2 via a hydrothermal approach to obtain mesoporous $\text{Fe}_3\text{O}_4@/\text{SiO}_2$ nanocomposites, which exhibit an approximately core-shell structure (Fig. 1E). Secondly, MMF resins are assembled through self-assembly with F127 as the template and methylolmelamines (products of melamine with paraformaldehyde), and then further deposited onto the surface of the $\text{Fe}_3\text{O}_4@/\text{SiO}_2$ nanocomposites. The diameters of particles after modification are larger (15–60 nm from Fig. 1C, F) than those of pristine magnetic composites, which could be attributed to the coverage of MMF resins.^{24,38,39} It needs to be noted that the size

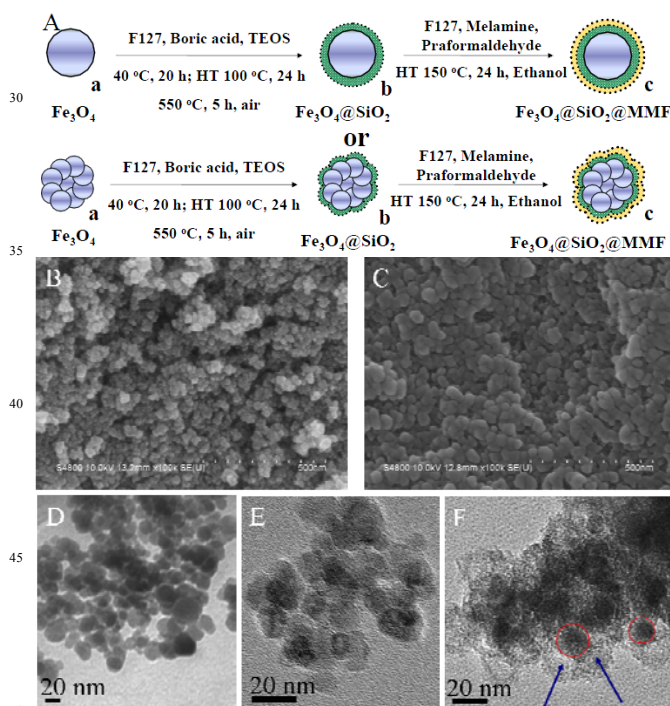


Fig. 1. (A) Schematic illustration of the formation of MMMF. (a) Fe_3O_4 nanospheres, (b) $\text{Fe}_3\text{O}_4@/\text{SiO}_2$ nanocomposites, (c) $\text{Fe}_3\text{O}_4@/\text{SiO}_2@/\text{MMF}$ nanoparticles (MMMF). (B) FESEM images of magnetic Fe_3O_4 nanospheres and (C) MMMF nanoparticles. (D) TEM images of Fe_3O_4 nanospheres, (E) $\text{Fe}_3\text{O}_4@/\text{SiO}_2$ nanocomposites and (F) MMMF nanoparticles.

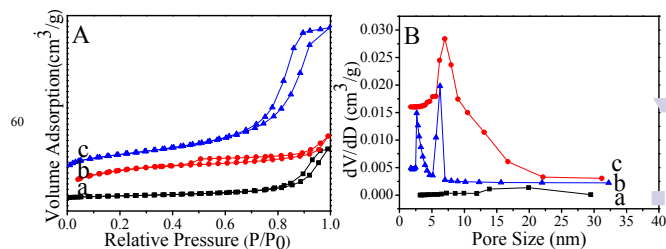


Fig. 2. (A) N_2 sorption isotherms and (B) pore size distributions of (a) magnetic Fe_3O_4 nanospheres (b) $\text{Fe}_3\text{O}_4@/\text{SiO}_2$ nanocomposites and (c) MMMF nanoparticles.

of the magnetic core of MMMF is smaller than that of most traditional magnetic oxides. Thus, we can obtain the magnetic adsorbent MMMF with thicker functional layer of MMF to avoid the decrease of adsorption capacity. On the other hand, it is difficult to synthesize monodisperse magnetic nanoparticles with a small size for their high surface area, high surface energy and the agglomeration property.⁴⁰ Thus, the TEM images show that the sample of Fe_3O_4 , $\text{Fe}_3\text{O}_4@/\text{SiO}_2$ and MMMF are agglomerated instead of perfectly monodispersed.

The N_2 sorption isotherms of both $\text{Fe}_3\text{O}_4@/\text{SiO}_2$ nanocomposites (Fig. 2A–b) and MMMF (Fig. 2A–c) exhibit a typical type IV curve with a hysteresis loop at 0.40–0.90 and 0.50–0.90, respectively, which confirm the presence of mesoporosity in these samples.⁴¹ Correspondingly, the pore size distributions of MMMF calculated using the BJH method are uniform and centered at 6.9 nm (Fig. 2B–c). Moreover, the N_2 sorption results also show that the MMMF nanoparticles possess a high BET surface area (393 m^2/g) and a relatively large pore volume (0.10 m^3/g). Interestingly, the BET surface area of MMMF is larger than that of the MMF resins (BET = 317 m^2/g , Table S1), which can be attributed to the mesoporous silica with a high surface area of 465 m^2/g .⁴²

The solid-state ^{13}C NMR spectra of MMMF clearly show four peaks at 46, 53, 153 and 163 ppm, respectively (Fig. 3). The signal at 153 ppm and the more intense signal at 163 ppm can be assigned to the triazine rings, whereas the strong peak at 53 ppm

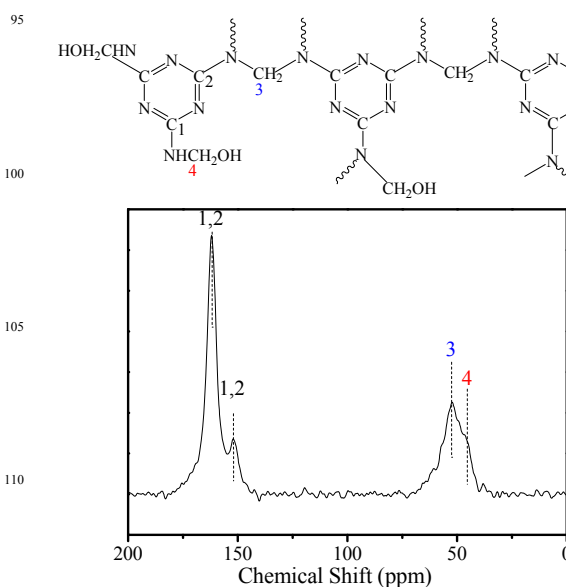


Fig. 3. ^{13}C NMR spectra of MMMFS sample.

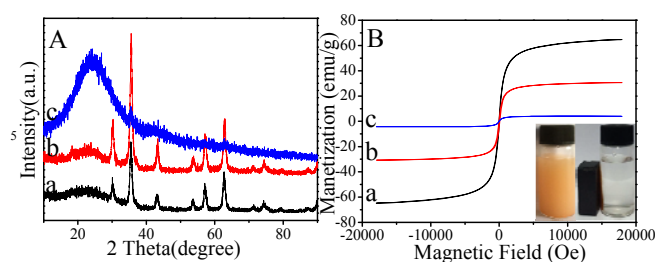


Fig. 4. (A) WXR D patterns and (B) room temperature magnetic hysteresis loops of (a) Fe_3O_4 nanospheres, (b) $\text{Fe}_3\text{O}_4@\text{SiO}_2$ nanocomposites, and (c) MMMF nanoparticles (optical photographs of MMMF dispersed in aqueous solution (left) and magnetic separation of MMMF within 1 min (right)).

is associated with the species of $-\text{NH}-\text{CH}_2-\text{NH}-$ and that at 46 ppm is related to the species of $-\text{NHCH}_2\text{OH}$.^{43,44} Moreover, the IR spectrum of Fe_3O_4 nanospheres, $\text{Fe}_3\text{O}_4@\text{SiO}_2$ nanocomposites and MMMF nanoparticles in the region of $400-4000\text{ cm}^{-1}$ are shown in Fig. S3. The typical absorption bands at 570 and 1382 cm^{-1} are attributed to the $\text{Fe}-\text{O}$ vibration and $\text{Fe}-\text{O}$ stretching, respectively.^{45,46} The strong bands at 1635 and 3440 cm^{-1} in Fig. S3B suggest the presence of hydrogen bonding, $-\text{OH}$ groups and H_2O molecules on the surface of $\text{Fe}_3\text{O}_4@\text{SiO}_2$ nanocomposites, respectively, which play a key role in adsorbing methylolmelamines or oligomers by hydrogen bond.^{45,46} In addition, the band at 1557 cm^{-1} indicates the existence of triazine rings in the sample.⁴⁷ The strong peak at 3440 cm^{-1} is attributed to the $-\text{NH}_2$ or $-\text{NH}$ stretching in the sample.⁴⁸ The chemical distributions of MMMF and MMMF/Cr samples were examined using EDS element mapping, and the results are presented in Fig. S4 and Fig. S5, respectively. The C, N, O, Fe, and Si elements are evenly distributed throughout the MMMF sample, and these uniformly distributed C, N and O elements can serve as active sites for trapping Cr ions.³⁵ Moreover, the Cr mapping of the MMMF/Cr sample shows that Cr is distributed uniformly in the sample, indicating the adsorption property of MMMF for Cr. In addition, the TGA results (Fig. S6) indicate that MMMF is thermally stable up to $300\text{ }^\circ\text{C}$ in a nitrogen atmosphere and that the residual mass of MMMF is higher than that of MMF, which can be attributed to the stable magnetic nanocomposites of $\text{Fe}_3\text{O}_4@\text{SiO}_2$.⁴⁹

The WXR D patterns of both magnetic Fe_3O_4 nanospheres (Fig. 4 A-a) and $\text{Fe}_3\text{O}_4@\text{SiO}_2$ nanocomposites (Fig. 4 A-b) show six well-resolved diffraction peaks ($2\theta = 30.1^\circ$, 35.5° , 43.1° , 53.4° , 57.0° , and 62.6°) marked by their indices ((220), (311), (400), (422), (511), and (440)), which agree well with the database information (JCPDS-01-1111),⁵⁰ demonstrating the successful synthesis of magnetic nanoparticles with high crystallinity. However, MMMF nanoparticles exhibit a relatively broader peak (Fig. 4 A-c) with only three typical peaks ($2\theta = 35.5^\circ$, 57.0° and 62.6°) of magnetic iron oxide Fe_3O_4 because of the small doping amount of magnetic composites of $\text{Fe}_3\text{O}_4@\text{SiO}_2$ in MMMF for the XRD diffraction.⁵¹ Moreover, the magnetic characterization results obtained using a VSM at room temperature indicate that magnetic Fe_3O_4 nanospheres, magnetic $\text{Fe}_3\text{O}_4@\text{SiO}_2$ nanocomposites and MMMF nanoparticles have a magnetization saturation of 64.4 , 30.8 , and 4.3 emu/g , respectively. The MMMF

nanoparticles can be separated easily from the solution under an external magnetic field within 1 min (Fig. 4 B inset photograph), which is very important for the recycling of adsorbents.^{52,53}

3.2 Adsorption property of MMMFS for Cr (VI)

The feasibility of MMMF nanoparticles as a magnetic recoverable adsorbent for wastewater treatment is demonstrated using Cr (VI) as a model compound. The effects of initial Cr (VI) concentration, temperature, and pH on adsorption property of MMMF are systematically investigated. Fig. 5 shows that the adsorption capacity of MMMF for Cr (VI) increases with the increase of initial Cr (VI) concentration. The adsorption rate is fast, and the maximum adsorption capacity is reached within approximately 5 to 10 min. The rapid adsorption performance of MMMF might be attributed to the functional groups, and the adsorbent is nanosized with a high surface area, which facilitates the contact between Cr (VI) and the active sites.⁵⁴ Moreover, the required equilibrium time for different initial concentrations shows no significant difference, indicating a strong interaction between the adsorbent and Cr (VI). However, the equilibrium time for some other adsorbents is much longer. For example, it has been shown that chitosan salt⁵⁵ and activated carbon⁵⁶ need approximately 50 and 285 h to reach the maximum adsorption capacity, respectively. More importantly, MMMF exhibits higher adsorption capacity than MMF for its much higher surface area, which may provide more active sites. In addition, the maximum adsorption capacity of MMMF is 41.7 , 65.5 , 101.9 , and 106.8 mg/g with the initial Cr (VI) concentrations of 45.7 , 83.3 , 113.9 , and 175.7 ppm , respectively (Table S2), suggesting that the adsorption capacity of MMMF for Cr (VI) increases rapidly at first with the increase of the initial Cr (VI) concentration and then remains almost unchanged. This is understandable because the amount of adsorbent is fixed, and thus the total number of available active sites is limited. Meanwhile, the magnetic $\text{Fe}_3\text{O}_4@\text{SiO}_2$ nanocomposites have no significant adsorption capacity for Cr (VI) (Table S3), indicating that the adsorption property is mainly dependent on the functional groups.

The effect of temperature ($20\text{ }^\circ\text{C}$, $25\text{ }^\circ\text{C}$, $30\text{ }^\circ\text{C}$, $35\text{ }^\circ\text{C}$, and $40\text{ }^\circ\text{C}$) on the adsorption capacity of MMMF for Cr (VI) is showed in Fig. 6. The adsorption capacity of MMMF for Cr (VI) first increases and then decreases slightly with the increase of temperature, with the maximum adsorption capacity being 41.6 mg/g ($20\text{ }^\circ\text{C}$), 41.7 mg/g ($25\text{ }^\circ\text{C}$), 41.2 mg/g ($30\text{ }^\circ\text{C}$), 41.2 mg/g

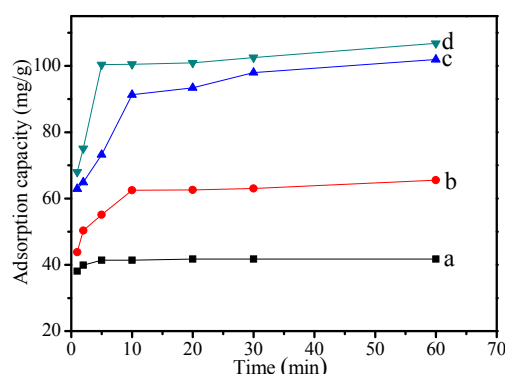


Fig. 5. Effect of initial Cr (VI) concentration ((a) 45.7 ppm , (b) 83.3 ppm , (c) 113.9 ppm , (d) 175.7 ppm) on the adsorption capacity of MMMF for Cr (VI).

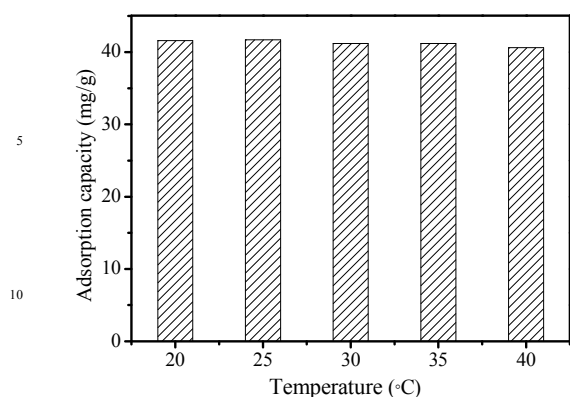


Fig. 6. Effect of temperature on the adsorption capacity of MMMF for Cr(VI).

(35 °C), and 40.6 mg/g (40 °C), respectively (Table S4). It is clear that the temperature has little effect on the adsorption property of MMMF for Cr(VI), indicating the strong interaction between the adsorbent MMMF and the adsorbed Cr(VI).

The pH of the aqueous solution could affect the forms of Cr ions and the number of protonated functional groups in the bonding sites of MMMF, which has a significant effect on the adsorption performance of MMMF (Fig. 7 and Table S5). The adsorption capacity of MMMF for Cr(VI) increases with the increase of pH until it reaches a maximum of 41.7 mg/g at pH 6.0 and then decreases thereafter. The adsorption of Cr is mainly caused by the electrostatic interactions between the protonated functional groups of MMMF and the anionic species of Cr. At a lower pH, the number of protonated functional groups increases with increasing pH, meanwhile, the dominant species of Cr are H_2CrO_4 and H_2CrO_7 , and the anionic species of HCrO_4^- , CrO_4^{2-} and $\text{Cr}_2\text{O}_7^{2-}$ are reduced, resulting in weak electrostatic interactions and thus a low adsorption capacity. With the increase of pH, the predominant species change into CrO_4^{2-} and the number of protonated functional groups of MMMF decreases, which could act as coordinating ligands for trapping Cr ions. However, if pH continues to increase, the surface of MMMF will be negatively charged, which will greatly reduce the electrostatic attraction between the adsorbent and Cr ions.^{35,57,58} This indicates that MMMF/Cr (MMMf adsorbed Cr(VI)) could be regenerated. Here, MMMF/Cr is subjected to 0.1 M NaOH to recover the adsorbed Cr ions. The desorption percentages of MMMF/Cr at different times are listed in Table S5. Interestingly,

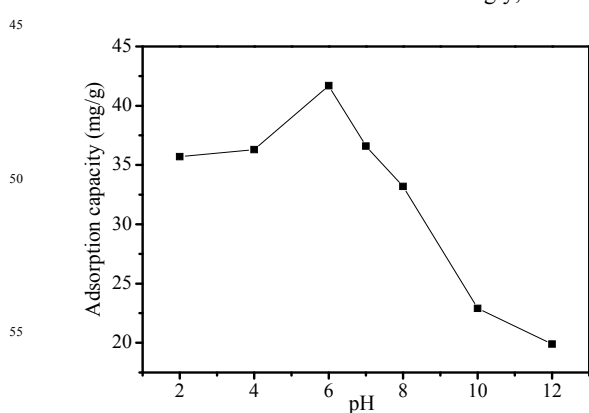


Fig. 7. Effect of pH on the adsorption capacity of MMMF for Cr(VI).

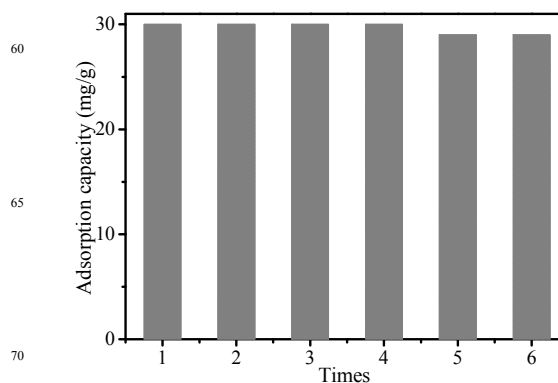


Fig. 8. Recovery of Cr(VI) and recycling of MMMF.

the adsorbent MMMF could be completely regenerated (100 %) within 1 min (Table S6). Moreover, the iron ions of MMMF can not be dissolved in the acid solution (Table S7), which is great value for expanding the application.

The reusability is a very important property for the industrial application of an adsorbent. Considering the low adsorption capacity of MMMF for Cr(VI) under basic conditions, 0.1 M NaOH solution was used for the elution of Cr(VI) from MMMF/Cr. In order to investigate the reusability of MMMF, the adsorption-desorption cycle was performed five times, and the results are presented in Fig. 8 and Table S8. It is evident that the variances of the adsorption capacity of MMMF are very small, indicating that MMMF exhibits good stability, regeneration ability and reusability.

Conclusions

Magnetically recoverable mesoporous melamine-formaldehyde nanospheres (MMMFS) have been successfully synthesized. As an efficient adsorbent for Cr(VI), MMMFS could quickly and effectively remove chromium ions from water within 5–10 min and more importantly, the recovery and regeneration of adsorbent is technical feasible. Furthermore, the adsorbent could be collected from water with a simple magnetic field and be reused for at least five times. The ease of synthesis coupled with the rapid and efficient adsorption properties made MMMFS an attractive adsorbent for water treatment and purification.

Acknowledgements

This work is supported by the National Natural Science Foundation of China (NO. 51463020) and the Fundamental Research Funds for the Central Universities (WD1315012).

Notes and references

- ^a Shanghai Key Laboratory of Advanced Polymeric Material, Key Laboratory for Ultrafine Materials of Ministry of Education, School of Materials Science and Engineering, East China University of Science and Technology, Shanghai 200237, China. Fax: (+86) 021 6425 3775; Tel: (+86) 021 6425 3353; E-mail: saxu@ecust.edu.cn
- ^b Chemical Experiment Center, School of Chemistry and Molecular Engineering, East China University of Science and Technology, Shanghai 200237, China
- † Electronic Supplementary Information (ESI) available: [details of any supplementary information available should be included here]. See DOI: 10.1039/b000000x/

- ‡ Footnotes should appear here. These might include comments relevant to but not central to the matter under discussion, limited experimental and spectral data, and crystallographic data.
1. N. L. Nemerow, A. Dasgupta, *Industrial and Hazardous Waste Treatment*, Van Nostrand Reinhold, New York, 1991.
 2. G. Tchobanoglous, L. B. Franklin, *Wastewater Engineering: Treatment, Disposal and Reuse*, McGraw Hill, Inc., New York, 1991.
 3. I. Ali, H. Y. Aboul-Enein, *Chiral Pollutants: Distribution, Toxicity and Analysis by Chromatography and Capillary Electrophoresis*, John Wiley & Sons: Chichester, UK, 2004.
 4. I. Ali, *Chem. Rev.*, 2012, **112**, 5073.
 5. E. A. Laws, *Aquatic Pollution: An Introductory Text*, John Wiley & Sons: New York, 2000.
 6. S.-H. Peng, W.-X. Wang, X. Li, Y.-F. Yen, *Chemosphere*, 2004, **57**, 839.
 7. S. Khan, Q. Cao, Y. M. Zheng, Y. Z. Huang, Y. G. Zhu, *Environ. Pollut.*, 2008, **152**, 686.
 8. A. Singh, R. K. Sharma, M. Agrawal, F. M. Marshall, *Food Chem. Toxicol.*, 2010, **48**, 611.
 9. M. Costa, *Toxicol. Appl. Pharmacol.*, 2003, **188**, 1.
 10. F. L. Petrilli, S. Flora, *Appl. Environ. Microbiol.*, 1977, **33**, 805.
 11. H. J. Gibb, P. S. J. Lees, P. F. Pinsky, B. C. Rooney, *Am. J. Indus. Med.*, 2000, **38**, 115.
 12. J. Fruchter, *Environ. Sci. Technol.*, 2002, **36**, 464A.
 13. Y. Xu, D. Zhao, *Water Res.*, 2007, **41**, 2101.
 14. M. Hua, S. Zhang, B. Pan, W. Zhang, L. Lv, Q. Zhang, *J. Hazard. Mater.*, 2012, **211–212**, 317.
 15. D. Mohan, C. U. Pittman Jr., *J. Hazard. Mater.*, 2006, **B137**, 762.
 16. V. M. Boddu, K. Abburi, J. L. Talbott, E. D. Smith, *Environ. Sci. Technol.*, 2003, **37**, 4449.
 17. D. Kratochvil, P. Pimentel, B. Volesky, *Environ. Sci. Technol.*, 1998, **32**, 2693.
 18. R. R. Patterson, S. Fendorf, *Environ. Sci. Technol.*, 1997, **31**, 2039.
 19. J. Pradhan, S. N. Das, R. S. Thakur, *J. Colloid. Interface. Sci.*, 1999, **217**, 137.
 20. P. Wang, I. M. C. Lo, *Water, Res.*, 2009, **43**, 3727.
 21. J. Hu, G. Chen, I. M. C. Lo, *Water, Res.*, 2005, **39**, 4528.
 22. J. Wang, G. Zhao, Y. Li, H. Zhu, X. Peng, X. Gao, *Dalton. Trans.*, 2014, **43**, 11637.
 23. M.-H. Liao, D.-H. Chen, *J. Mater. Chem.*, 2002, **12**, 3654.
 24. X. Liu, Y. Guan, Z. Ma, H. Liu, *Langmuir*, 2004, **20**, 10278.
 25. Y.-C. Chang, D.-H. Chen, *J. Colloid. Interface. Sci.*, 2005, **283**, 446.
 26. L. C. A. Oliveira, D. I. Petkowicz, A. Smaniotto, S. B. C. Pergher, *Water, Res.*, 2004, **38**, 3699.
 27. X. Chen, K. F. Lam, Q. Zhang, B. Pan, M. Arruebo, K. L. Yeung, *J. Phys. Chem. C*, 2009, **113**, 9804.
 28. N. Andersson, R. W. Corkery, P. C. A. Alberius, *J. Mater. Chem.*, 2007, **17**, 2700.
 29. M. Arruebo, W. Y. Ho, K. F. Lam, X. Chen, J. Arbiol, J. Santamaria, K. L. Yeung, *Chem. Mater.*, 2008, **20**, 486.
 30. J. Liu, S. Z. Qiao, Q. H. Hu, G. Q. Lu, *Small*, 2011, **7**, 425.
 31. L. Zhou, S. Pan, X. Chen, Y. Zhao, B. Zou, M. Jin, *Chem. Eng. J.*, 2014, **257**, 10.
 32. R. Kaur, A. Hasan, N. Iqbal, S. Alam, M. K. Saini, S. K. Raza, *J. Sep. Sci.*, 2014, **37**, 1805.
 33. Y. Wang, B. Li, L. Zhang, P. Li, L. Wang, J. Zhang, *Langmuir*, 2012, **28**, 1657.
 34. Z. Lv, C. Liang, J. Cui, Y. Zhang, *RSC Adv.*, 2015, **5**, 18213.
 35. R. V. Mehta, R. V. Upadhyay, S. W. Charles, C. N. Ramchand, *Biotechnol. Tech.*, 1997, **11**, 493.
 36. J. Yang, F. Zhang, W. Li, D. Gu, D. Shen, J. Fan, W.-X. Zhang, D. Zhao, *Chem. Commun.*, 2014, **50**, 713.
 37. H. Yu, M. Chen, P. M. Rice, S. X. Wang, R. L. White, S. Sun, *Nano Lett.*, 2005, **5**, 379.
 38. Y. Pang, G. Zeng, L. Tang, Y. Zhang, Y. Liu, X. Lei, Z. Li, J. Zhang, Z. Liu, Y. Xiong, *Chem. Eng. J.*, 2011, **175**, 222.
 39. R. Hao, R. Xing, Z. Xu, Y. Hou, S. Gao, S. Sun, *Adv. Mater.*, 2010, **22**, 2729.
 40. M. Kruk, M. Jaroniec, *Chem. Mater.*, 2003, **15**, 2942.
 41. Y. Fang, G. Zheng, J. Yang, H. Tang, Y. Zhang, B. Kong, Y. Lv, C. Xu, A. M. Asiri, J. Zi, F. Zhang, D. Zhao, *Angew. Chem. Int. Ed.*, 2014, **53**, 5366.
 42. K. Kailasam, Y.-S. Jun, P. Katekomol, J. D. Epping, W. H. Hong, A. Thomas, *Chem. Mater.*, 2010, **22**, 428.
 43. M. G. Schwab, B. Fassbender, H. W. Spiess, A. Thomas, X. Feng, K. Müllen, *J. Am. Chem. Soc.*, 2009, **131**, 7216.
 44. W. Ma, F.-Q. Ya, M. Han, R. Wang, *J. Hazard. Mater.*, 2007, **143**, 296.
 45. Z. Liu, H. Wang, C. Liu, Y. Jiang, G. Yu, X. Mu, X. Wang, *Chem. Commun.*, 2012, **48**, 7350.
 46. Z. Lv, Q. Sun, X. Meng, F.-S. Xiao, *J. Mater. Chem. A*, 2013, **1**, 8630.
 47. M. X. Tan, Y. Zhang, J. Y. Ying, *ChemSusChem.*, 2013, **6**, 1186.
 48. J. Wang, W. Li, F. Wang, Y. Xia, A. M. Asiri, *Nanoscale*, 2014, **6**, 3217.
 49. N. A. Travlou, G. Z. Kyzas, N. K. Lazaridis, E. A. Deliyanni, *Langmuir*, 2013, **29**, 1657.
 50. J. Cha, J. S. Lee, S. J. Yoon, Y. K. Kim, J.-K. Lee, *RSC Adv.*, 2013, **3**, 3631.
 51. H. Deng, X. Li, Q. Peng, X. Wang, J. Chen, Y. Li, *Angew. Chem. Int. Ed.*, 2005, **117**, 2842.
 52. J. Gao, X. Ran, C. Shi, H. Cheng, T. Cheng, Y. Su, *Nanoscale*, 2013, **5**, 7026.
 53. M. X. Tan, Y. N. Sum, J. Y. Ying, Y. Zhang, *Energy. Environ. Sci.*, 2013, **6**, 3254.
 54. V. A. Spinelli, M. C. M. Laranjeira, V. T. Fávere, *React. Funct. Polym.*, 2004, **61**, 347.
 55. M. Pérez-Candela, J. M. Martín-Martínez, R. Torregrosa-Maciá, *Wat. Res.*, 1995, **29**, 2174.
 56. H.-J. Park, L. L. Tavlarides, *Ind. Eng. Chem. Res.*, 2008, **47**, 3401.
 57. Z. Ren, D. Kong, K. Wang, W. Zhang, *J. Mater. Chem. A*, 2014, **2**, 17952.
 - 58.

Magnetically recoverable mesoporous melamine–formaldehyde nanoparticles as an efficient adsorbent for hexavalent chromium removal

